ACS APPLIED MATERIALS & INTERFACES

Research Article

www.acsami.org

Three-Dimensional Macroporous Polypyrrole-Derived Graphene Electrode Prepared by the Hydrogen Bubble Dynamic Template for Supercapacitors and Metal-Free Catalysts

Xiaoqing Yang, Anran Liu,* Yuewu Zhao, Huijia Lu, Yuanjian Zhang, Wei Wei, Ying Li, and Songqin Liu*

Jiangsu Province Hi-Tech Key Laboratory for Bio-medical Research, School of Chemistry and Chemical Engineering, Southeast University, Nanjing, Jiangsu 211189, P. R. China

Supporting Information

ABSTRACT: We report a general method for the fabrication of three-dimensional (3D) macroporous graphene/conducting polymer modified electrode and nitrogen-doped graphene modified electrode. This method involves three consecutive steps. First, the 3D macroporous graphene (3D MG) electrode was fabricated electrochemically by reducing graphene oxide dispersion on different conducting substrates and used hydrogen bubbles as the dynamic template. The morphology and pore size of 3D MG could be governed by the use of surfactants and the dynamics of bubble generation and departure. Second, 3D macroporous graphene/polypyrrole (MGPPy) composites were constructed via directly electropolymerizing pyrrole monomer onto the networks of 3D MG. Due to the benefit of the good conductivity of 3D MG and pseudocapacitance of PPy, the composites manifest outstanding area specific capacitance of 196 mF cm^{-2} at a current density of 1 mA cm^{-2}. The symmetric supercapacitor device assembled by the composite materials had a good capacity property. Finally, the nitrogen-doped MGPPy (N-MGPPy or MGPPy-X) with 3D macroporous nanostructure and well-regulated nitrogen doping was prepared via thermal treatment of the composites. The resultant N-MGPPy electrode was explored as a good electrocatalyst for the oxygen reduction reaction (ORR) with the current density value of 5.56 mA cm^{-2} (−0.132 V vs Ag/AgCl). Moreover, the fuel tolerance and durability under the electrochemical environment of the N-MGPPy catalyst were found to be superior to the Pt/C catalyst.

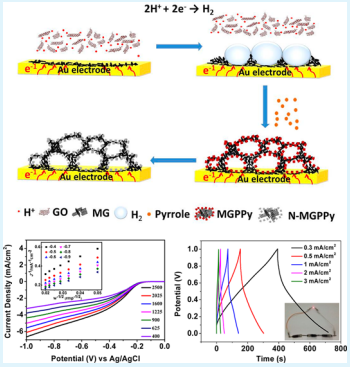

KEYWORDS: *hydrogen bubble template, elcctrochemical reduced graphene oxide, graphene modified electrode, graphene/polypyrrole composites, nitrogen-doped, supercapacitors, oxygen reduction reaction*

1. INTRODUCTION

Graphene is a single atom layer 2D sheet of sp^2 hexagonal carbons with outstanding electrical and thermal properties,[1,2] great mechanical strength,[3] and large surface area.[4] In particular, graphene, heteroatom-doped graphene, and graphene-based composites have been widely studied as promising electrode materials for supercapacitors, oxygen reduction reaction, lithium-ion batteries, and electroanalysis.[5−16] Large electrode surface area, more active sites of reaction, and fast electrolyte transport near the electrode surface of the graphene are required for electrodes in each of the above electrochemical applications, in order to obtain a high rate of electrochemical reaction. Typically, graphene-modified electrodes were prepared by drop-casting of the well dispersed graphene oxide or reduced graphene oxide solution on an underlying support electrode.[17] However, due to strong $\pi-\pi$ interaction between graphene sheets, they tend to stack with each other in a parallel arrangement, forming graphite-like powders with compact layered structures when processed into bulk electrode materials. The aggregation of graphene will hinder the rapid electrolyte diffusion and reduce the surface area of the electrode.[18] Graphene-modified electrodes prepared by drop-casting often suffer from disadvantages of low electrical conductivity, small electrode surface area, and unstable mechanical property. Moreover, electrochemically inactive polymer binders and/or conductive additives are usually needed to combine these graphite-like graphene powders into practical electrodes, which not only complicates the electrode preparation process but also introduces additional loss in the electrochemical performance.[19] Self-assembly of nanoscale graphene into monolithic macroscopic materials with three-dimensional (3D) porous networks can largely translate the properties of individual graphene into the resulting macrostructures and simplify the processing of graphene materials.[20−24] Considerable template-directed synthesis methods are used to fabricate 3D graphene-based structure, including hard-template and soft-template methods. The hard-template process must remove the template such as nickel foam, silica, or polystyrene which may destroy the morphology and structure.[25−30] Compared with the hard-template method, the soft-template method has unique advantages,[31,32] such as being simple and economic while avoiding harsh experimental conditions, which can be realized

Received: August 27, 2015
Accepted: October 12, 2015
Published: October 12, 2015

DOI: 10.1021/acsami.5b07982
ACS Appl. Mater. Interfaces 2015, 7, 23731−23740

by means of chemical and electrochemical methods.[33−36] Herein, we first develop a facile method to guide graphene oxide assembling on different conducting substrates such as metal foil, carbon paper, and ITO glass with the assistance of the hydrogen bubble template. Subsequently, pyrrole monomer is electropolymerized on the networks of 3D macroporous graphene (MG), yielding graphene-based 3D macroporous graphene/polypyrrole (MGPPy) composite materials. After annealing at high temperature, the nitrogen-doped MGPPy (N-MGPPy or MGPPy-X) was synthesized with 3D macroporous nanostructure and a high percentage of nitrogen. Finally, the application of the composite materials prepared with our method was discussed. The obtained MGPPy and N-MGPPy modified electrodes with three-dimensional (3D) macroporous networks can be used for supercapacitors and catalysts for oxygen reduction reaction.

2. EXPERIMENTAL SECTION

2.1. Materials. Lithium perchlorate ($LiClO_4$, 98%), sodium dodecylbenzenesulfonate (SDBS, 95%), and pyrrole were purchased from Aladdin. Graphene oxide (GO) was prepared by oxidation of natural graphite powder (325 mesh) according to a modified Hummers' method.[37] (As shown in Figure S1, TEM and AFM results demonstrated that single layer GO was prepared.) Commercial 20 wt % Pt/C (HiSPECTM 3000) was from Johnson Matthey. Other chemicals such as sulfuric acid (H_2SO_4, 98%), hydrochloric acid (HCl, 36%), potassium chloride, potassium hydroxide, and ethanol were from Sinopharm Chemical Reagent Co. Ltd. (China). All the reagents were of analytical grade and used as received. All solutions used in the experiments were freshly prepared with ultrapure water having a resistivity of 18.2 MΩ cm^{-1} (Nanjing Baocheng Biotechnology CO. Ltd., China).

2.2. Preparation of 3D Macroporous Graphene (MG) Materials. The 3D MG materials were prepared with a chronoamperometry method in a GO (3 mg/mL) aqueous dispersion consisting of 0.1 M $LiClO_4$, 50 μM H_2SO_4, and SDBS at different deposition times (s) (nMG, n is the time of deposition) and different potentials such as −0.8, −1.0, and −1.2 V.[38] A saturated calomel electrode (SCE), Pt foil, and Au (1 × 1.5 cm^2) foil were used as the reference, counter, and working electrode, respectively. Finally, the MG electrodes were washed repeatedly to remove the remaining purities and immersed in ultrapure water to prevent the collapse of the porous structure caused by drying in air.

2.3. Preparation of 3D Macroporous Graphene/Polypyrrole (MGPPy) Materials. The composite materials were prepared by electropolymerizing 0.1 M pyrrole, aqueous, containing 0.1 M SDBS at the potential of +0.75 V for different times with 3D prepared-MG as the working electrode. The amount of deposited PPy was controlled by deposition time (s) (nMGmPPy, m is the time of deposition). The as-prepared samples were washed repeatedly and immersed in ultrapure water.

2.4. Preparation of 3D Nitrogen Doped Graphene/Polypyrrole (N-MGPPy) Materials. 3D N-MGPPy electrodes were prepared by simple heat treatment of the as-prepared MGPPy composites in a nitrogen atmosphere at different heating temperatures such as 600, 800, and 1000 °C for 2 h. Since the oxygen reduction activity is strongly influenced by the heat treatment temperature, the resultant samples were termed MGPPy-X (X is the annealing temperature) for further studies of electrochemical oxygen reduction reaction (ORR) activity.

2.5. Apparatus. The morphologies of electrode materials were studied by using a field-emission scanning electron microscope (SEM, JSM-7001F, JEOL, Japan) and a FEI TECNAI TF20 transmission electron microscope (TEM, JEM-2010, JEOL, Japan). Energy dispersive X-ray spectra (EDS) were taken on a field-emission scanning electron microscope (SEM, JSM-7001F, JEOL, Japan). Raman spectra were recorded on an Invia Raman spectrometer (Renishaw) with a 514 nm laser. X-ray photoelectron spectroscopy (XPS) was performed by a PHI5000 VersaProbe (Ulvac-Phi, Japan) system with a monochromic Mg Kα radiation. X-ray diffraction (XRD) was performed on a D8 (Advance, Bruker, Germany), and the data were collected in the 2θ range of 10−70° at a step size of 0.02°. Brunauer−Emmett−Teller (BET) surface areas were investigated by NobaWin (Quantachrom, USA). Thermogravimetric (TG) analysis was performed on the SDT-Q600 thermal analyzer (TA Instruments, USA) in an N_2 atmosphere at a heating rate of 20 °C min^{-1} with temperature ranging from 50 to 850 °C.

2.6. Electrochemical Tests. *2.6.1. Electrochemical Supercapacitor Properties of MG and MGPPy.* The electrochemical performances of MG and MGPPy were tested by cyclic voltammetry (CV), galvanostatic charge−discharge (GCD), and electrochemical impedance spectra (EIS). All experiments were carried out in a three electrode system with Pt foil as the counter electrode, a SCE as the reference electrode, and MG or MGPPy as the working electrode. The potential range for CV measurements and GCD tests were −0.8 to 0.2 V using a CHI 660C Potentiostat (CH Instruments, Inc.). The EIS measurements were performed over the frequency range from 10^5 to 10^{-1} Hz at the amplitude of the sinusoidal voltage of 5 mV using Princeton Applied Research. The cycle life tests were conducted by GCD measurements with a constant current density of 1 mA cm^{-2} for 500 cycles. The specific capacitances of composite electrodes were evaluated in area units (mF cm^{-2}). The area specific capacitances (C_A) were calculated by using the equations $C_A = I\Delta t/A\Delta v$, where I is the constant discharge current, Δt is the discharge time, A is the area of the Au foil for the electrodeposition, and Δv is the voltage drop upon discharging.

2.6.2. Fabrication of Symmetrical Supercapacitor Device. The symmetrical supercapacitor was assembled using 120MG600PPy carbon paper electrode (1.5 cm^2) and Au electrode with a separator (NKK separator; Nippon Kodoshi Corporation, Kochi, Japan) sandwiched between the two electrodes. A KCl (1 M) aqueous solution was used as the electrolyte. To avoid leakage of the electrolyte, the entire device was sealed by two pieces of PET membranes with a small part of electrode kept outside. Figure S2 shows the schematic illustration of the asymmetric supercapacitor configuration.

2.6.3. Electrochemical Oxygen Reduction Properties of MGPPy-X. Electrochemical measurements were also conducted with a three electrode electrochemical cell using a CHI700 electrochemical workstation (CH Instruments, China) and rotating ring disk electrode (RRDE-3A, Japan). Pt foil, Ag/AgCl, and glassy carbon electrode (GCE) with a diameter of 3 mm were used as the counter electrode, reference electrode, and working electrode. For electrode preparation, MGPPy and MGPPy-X suspension in ethanol (2 mg/mL) were prepared by adding the prepared sample to ethanol under sonication. A 10 μL portion of the suspension was then dropped onto the surface of a prepolished glassy carbon electrode (GCE), followed by dropping 5 μL of nafion (0.05% in ethanol) as a binder. The activity of the electrocatalyst was evaluated by the cyclic voltammetry and liner sweep voltammetry techniques in an aqueous solution of 0.1 M KOH, which was bubbled with O_2 or N_2 for 30 min and maintained with the same atmosphere during the measurements.

3. RESULTS AND DISCUSSION

3.1. Microstructure and Morphology. The synthesis approach of N-MGPPy is divided into 3 steps and illustrated in Scheme 1. First, the macroporous reduced graphene oxide electrode can be prepared by electrodepositing a 3 mg/mL GO mixture, aqueous, on a conducting electrode (e.g., Au) at an applied potential of −1.2 V for 120 s with hydrogen bubbles as templates. As shown in Figure S3, MG deposited under a potential of −1.2 V had better porous morphology than that deposited under a potential of −1.0 V. Thus, the potential of −1.2 V was chosen for electrodeposition of graphene oxide. The XPS survey spectra shown in Figure S4 demonstrated that graphene was largely reduced after electrodeposition. Then, the

DOI: 10.1021/acsami.5b07982
ACS Appl. Mater. Interfaces 2015, 7, 23731−23740

Scheme 1. Schematic Illustration of the Formation Process of the 3D MG, MGPPy, and N-MGPPy

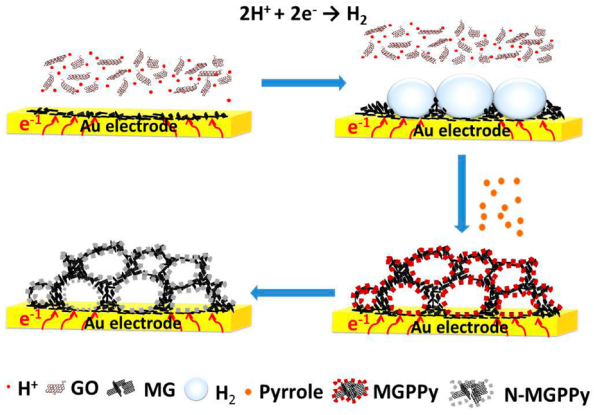

as-prepared MG was conductive and highly accessible for electrolyte and thus can be used as porous electrode into which pyrrole can be electropolymerized and produced graphene-based composite materials. The synergy effects make the MGPPy composite materials exhibit a high area specific capacitance, good capacitance retention, and excellent cycling stability as supercapacitors. The obtained materials were further pyrolyzed at a high temperature to form N-doped graphene electrode, which has a highly porous interconnected network, conductive multiplexed channels, and high pyrrolic nitrogen content. Thermal gravimetric analysis (TGA) of MGPPy composites was also studied in Figure S5. From 250 to 550 °C, MGPPy showed about 28% mass loss, possibly due to the release of its functional groups such as −OH and −COOH. At 500 °C, MGPPy still kept about 40% weight residual, indicating the graphitization of MGPPy. The N-MGPPy delivered a promising electrochemical catalytic activity of oxygen reduction reaction. SEM images of MG structure at different magnifications (Figure 1A,B) clearly show a macroporous structure throughout the entire sample. The pore sizes were arranged from 20 to 50 μm which agreed with the hydrogen bubble size of Qu's work.[39] As shown in the cross-section SEM images,

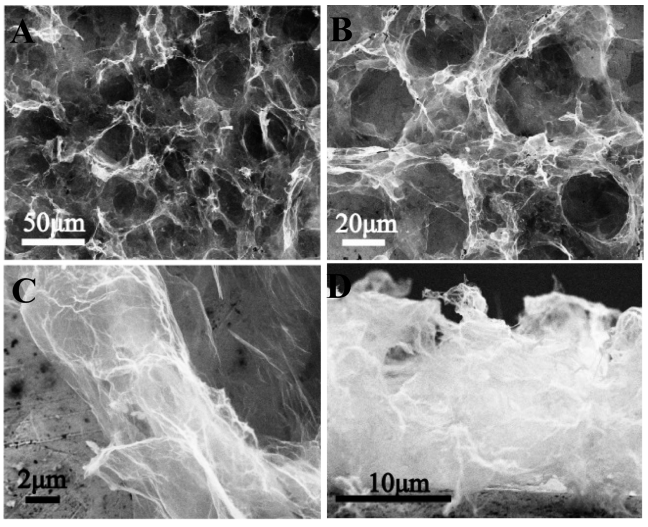

Figure 1. (A, B, C) Top-view scanning electron microscope images of the 3D MG electrode with low and high magnifications. (D) Cross-sectional scanning electron microscope image of the 3D MG electrode.

graphene plates formed the wall of the MG structure and were nearly vertical to the surface of the Au electrode (Figures 1C,D and S6). The thickness of the MG was about 14 μm.

Figure 2 shows the preparation process of these composite materials. At the beginning of the electrodepostion process, H^+

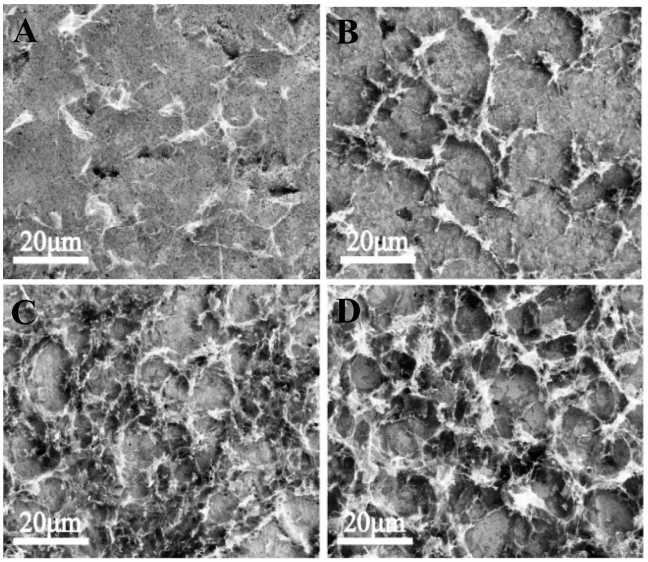

Figure 2. Scanning electron microscope images of the 3D MG electrodes with different deposition times (A) 10 s, (B) 30 s, (C) 60 s, and (D) 90 s.

and GO were both reduced at the electrode surface for the negative potential. GO was reduced and formed the graphene basal layer, while H^+ was reduced to hydrogen gas and formed gas bubbles. SDBS and GO are surfactants, and they can also stabilize gas bubbles on the working electrode surface.[40] Actually, we observed that a large amount of hydrogen gas bubbles was released from the surface of the working electrode during electrochemical deposition after 10 s (Figure 2A). These hydrogen gas bubbles were used as the dynamic template[41] for the growth of MG. GO was reduced and stacked in the interstitial spaces between the hydrogen bubbles and further generated the walls of porous structure. When deposition time was 90 s (Figure 2D), the thickness of MG increased to about 8.4 μm including the 400 nm basal graphene layer and 8.3 μm wall of the porous structure (Figure S6c). In this work, SDBS (anion surfactant) has also been used to stabilize the hydrogen bubble in the dynamic template system, altering the surface tension of the sol/gas and protecting the bubbles from coalescence. With the increase of surfactant concentration, the pore of the MG turned to become bigger and deeper (Figure S7). When the concentration of surfactant was under 50 mM or exceeded 300 mM, the bubble was generated faster and could not maintain the tension of sol/gas. Hydrogen bubbles merged into larger ones and departed; thus, they can not be the template for the formation of MG material. Since the bubble size and formation were affected by the concentration of surfactant, the pore size and morphology of the porous MG were tuned by the concentration of SDBS. This phenomenon is in full agreement with the results reported previously by other researchers.[35]

The as-prepared MG was conductive and highly accessible for the electrolyte; thus, it can be used as porous electrode into which other materials can be deposited using the electro-

DOI: 10.1021/acsami.5b07982
ACS Appl. Mater. Interfaces 2015, 7, 23731−23740

chemical method, producing graphene-based composite materials.[42] Here, the electrochemical polymerization of pyrrole monomer on MG networks was conducted in an electrolyte solution consisting of 0.1 M SDBS and 0.1 M pyrrole aqueous at the potential of +0.75 V. SDBS was used as a surfactant for dissolving the pyrrole monomer in the aqueous phase and also as a supporting electrolyte for improving the conductivity of the electrolyte solution.[43] N-MGPPy was prepared by the annealing treatment of the MGPPy composite. Figure 3A,B show the SEM images of MGPPy and MGPPy-800 composite material. Comparing the SEM of MG, the structure of MGPPy has no obvious change, the surface became rougher, and the wall became thicker with the addition of PPy (Figure S8). The pore diameters of MGPPy-800 became narrow due to the fact that the obtained sheets became thinner and more carbonized PPy on the surface of GO was decomposed in a high temperature annealing process (Figure S9). BET showed MG, MGPPy, and MGPPy-800 macroporous structure and the specific surface of 101.52, 40.11, and 102.17 $m^2\ g^{-1}$ (Figure S10), respectively. The introduction of PPy into the framework of MG led to a decreased specific surface area. However, after high temperature treatment, MGPPy-800 restored the initial specific surface, which agreed with the SEM images (Figure 3B). As seen in Figure 3C,D, the N and C heteroatoms distributed uniformly throughout the surfaces of MGPPy-800. After heat treatment, the 3D porous structure was well maintained, and the sheets of the MGPPy-800 featured abundant crumpled wrinkles (Figure 3B).

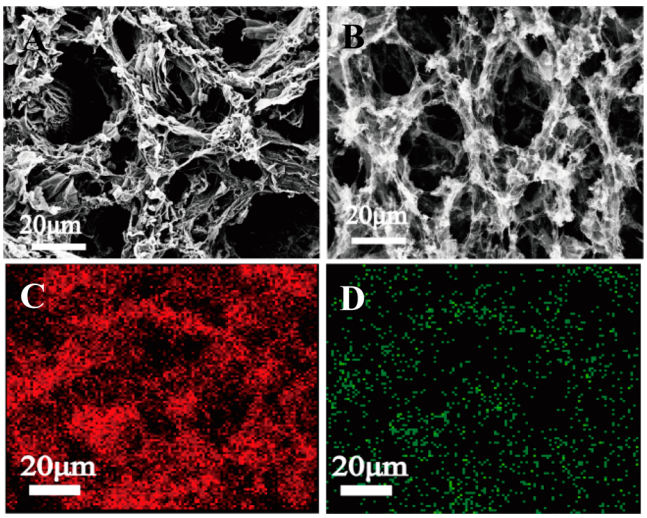

Figure 3. Scanning electron microscope images of 3D (A) MGPPy and (B) MGPPy-800 composite electrodes. EDS elemental mapping analysis of MGPPy-800 (C) carbon and (D) nitrogen.

Raman spectroscopy is one of the most useful methods to determine the defects, ordered and disordered structures, and the layers of graphene. As shown in Figure 4A, Raman spectra of GO and MG had two representative bands at 1345 cm^{-1} (D band) and 1580 cm^{-1} (G band) and the intensity ratios of D and G bands (I_D/I_G) for MG were calculated to be 1.73 which was higher than 0.99 for GO. This result suggested the reduction of GO to MG. For MGPPy composite, apart from the typical D and G bands of MG, the other prominent peaks at 977, 1048, and 1248 cm^{-1}, which are the characteristic peaks of PPy, suggested the successful deposition of PPy on the MG networks.[44] For MGPPy-800, the intensity ratio of the D to the G peak (I_D/I_G) larger than MG or MGPPy and the typical peak of PPy disappeared. It suggested the structural disorder was increased, which was ascribed to the doping of nitrogen into the graphene sheets.[45] Moreover, Figure S11 shows the Raman spectroscopy of N-MGPPy at different temperatures. Figure 4B showed the XRD patterns of MG, PPy, MGPPy, and MGPPy-800. The spectrum of pure PPy depicted a broad peak in the region of 2θ = 15−25°, which indicated that the polymer is basically amorphous, and the diffraction peak of MG was 23°, showing the electrochemical reduction of GO. Meanwhile, MG is also amorphous as in the previous work.[46] After electrodeposition of PPy, the diffraction peak at about 2θ = 20° in MGPPy was the overlap of amorphous PPy and loosely packed graphene sheets, and with the introduction of the nitrogen species into graphene lattice via thermal annealing of the resultant MGPPy to MGPPy-800, the pore diameters of these samples became narrow with increasing pyrolysis temperature.

XPS spectra were performed to identify the composition and nitrogen doping states of the obtained MGPPy and MGPPy-800 samples. As shown in Figure 5A, XPS analysis revealed the presence of C 1s, N 1s, and O 1s in the above three materials. Compared with the MGPPy, the peak intensity of MGPPy-800 of N and O was decreased, indicating that thermal annealing decomposed PPy on the surface of MG. Figure 5B shows the N 1s spectra of the MGPPy and MGPPy-800, where fitting lines indicate the bonding states of the doped nitrogen in the two composites. Generally, the doped nitrogen in MGPPy shows three component peaks originating from −N═, N−H, and $-N^+$ appearing at 398.3 ± 0.1, 400.3 ± 0.3, and 401.7 ± 0.3 eV,

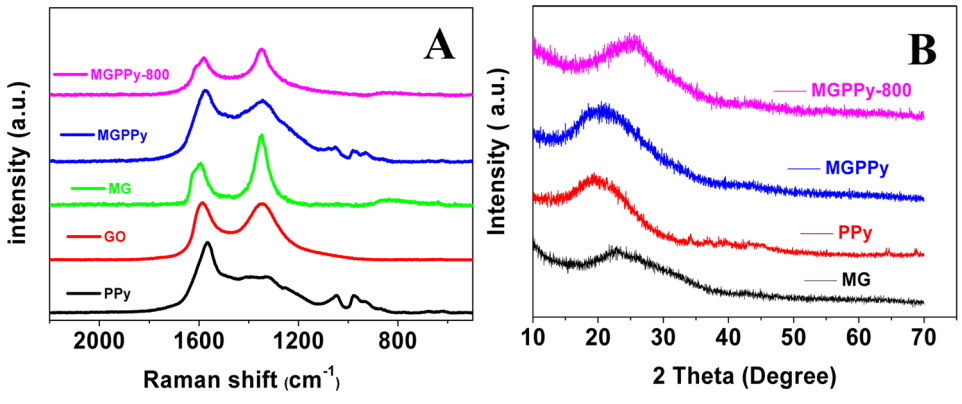

Figure 4. Raman (A) and XRD (B) spectra of MG, MGPPy, and MGPPy-800.

DOI: 10.1021/acsami.5b07982
ACS Appl. Mater. Interfaces 2015, 7, 23731−23740

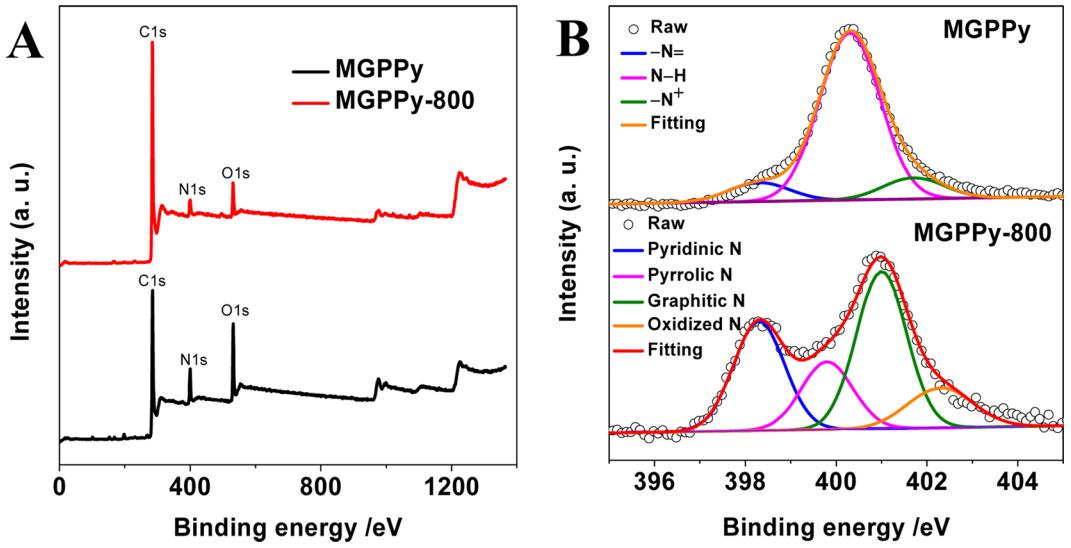

Figure 5. XPS survey spectra (A) and N 1s spectra (B) of the MGPPy and MGPPy-800.

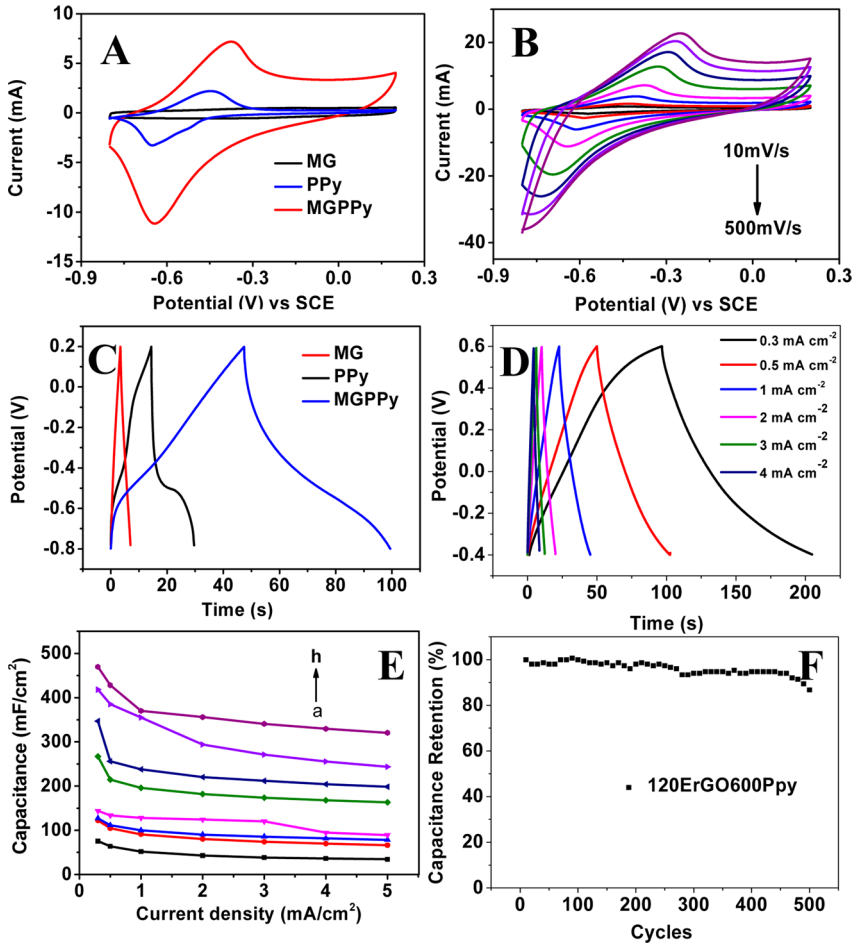

Figure 6. (A) CV curves of MG, PPy, and MGPPy composite potential from −0.8 to 0.2 V in 1 M KCl. (B) CV curves of MGPPy composite at various scan rates (10 to 500 mV s^{-1}). (C) Charge−discharge curves of MG, PPy, and 120MG120PPy (current density, 0.5 mA cm^{-2}). (D) Charge−discharge curves of 120MG120PPy at different current densities. (E) Areal capacitance of MGPPy composite with different PPy mass loadings with respect to discharge current (120MG120PPy, 120MG240PPy, 120MG360PPy, 120MG480PPy, 120MG600PPy, 120MG900PPy, 120MG1200PPy, and 120MG1500PPy). (F) Cycling performance of the 120MG600PPy for charging and discharging at a current density of 1 mA cm^{-1}.

respectively.[47] It might be due to the $\pi-\pi$ stacked between the PPy and MG layers, which is in accordance with the Raman results (Figure 4A). The doped nitrogen in MGPPy-800 existed in four forms, i.e., pyridinic−N (28.52%), pyrrolic−N (17.88%), graphitic−N (40.35%), and oxidized−N (13.24%) with the corresponding binding energy (B.E.) peaks at 398.3 ±

DOI: 10.1021/acsami.5b07982
ACS Appl. Mater. Interfaces 2015, 7, 23731−23740

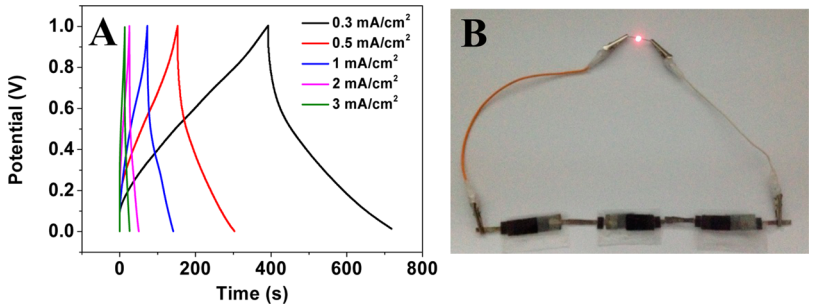

Figure 7. (A) Galvanostatic discharge−charge curves at current densities from 0.3 to 3 mA/cm^2. (B) Photographs of commercial red LED powered by our devices with three in series.

0.3, 399.8 ± 0.3, 401 ± 0.3, and 402.9 ± 0.3 eV,[48−50] respectively. It indicated that eletrodeposition of pyrrole and thermal annealing formed the MGPPy-800 composite, which clearly supports the presence of carbonized PPy on the graphene sheets prior to the annealing process. The MGPPy-800 had 40.35% graphitic N, which was higher than MGPPy because the N atoms in PPy can be easily converted to graphitic−N with the high temperature, and the pyrrolic−N percentage decreased while the pyridinic−N percentage increased monotonically, indicating a transformation from pyrrolic−N to pyridinic−N.[49] Raman spectroscopy further confirmed the incorporation of nitrogen into the graphene lattice.

3.2. Electrochemical Performance. *3.2.1. Supercapacitor.* Due to their high specific surface area, excellent electronic conductivity, and the benefit of the redox reactions, the resultant MGPPy modified electrode can be used as the working electrode of the supercapacitor. Figure 6A illustrates the CV of MG, PPy, and MGPPy composite electrode with a voltage range from −0.8 to 0.2 V. MG (specific surface area of 101.523 m^2 g^{-1}) showed a rectangular CV curve, indicating ideal capacitive behavior. PPy showed an obvious redox peak curve as a result of the doping−dedoping process. In contrast, the CVs of MGPPy exhibited much larger rectangular areas than the CVs of the pure MG and PPy. This observation can be explained as follows. First, the electrodeposition of PPy onto MG greatly improved the specific capacitance of the composite by forming a porous structure which has high specific surface area (SSA). The Brunauer−Emmett−Teller specific surface area test (BETSSA) showed that the SSA of MGPPy (40.1 m^2 g^{-1}) was much higher than that of the pure PPy film (1.3 m^2 g^{-1}).[46] Second, the pseudocapacitance of PPy in the composite film was enhanced by its highly conductive 3D graphene network, which favors the redox reaction of the PPy component. PPy in its neutral state is an insulator; thus, the MGPPy electrode had a large internal resistance as it is fully discharged. The MGPPy showed redox peak shape with a larger area benefit of the synergy effect of MG and PPy. Figure 6B shows the CV curves of MGPPy at various scan rates ranging from 10 to 500 mV s^{-1}. With the increased scan rate, the shape of the curve gradually deviated from the original redox peaks. In addition, the shift of the current peaks with the change in the scan rate demonstrates that the diffusion or intercalation of ions in the PPy film is a sluggish process. The ion in the electrolyte can reach everywhere at a low scan rate, resulting in a redox reaction that can occur at low scan rate. However, with the increase of the scan rate, the redox reaction degree between the electrolyte and PPy decreased; the ion cannot reach the surface of PPy, resulting in deviation from the original peak shape. As Figure 6B illustrates, the shape of the CV curve remained unchanged up to 500 mV s^{-1}, and the size of the CV became bigger with the increase of scan rate, revealing great capacitance and good ion response of the composite. To investigate the charge capacity of the samples, a charge−discharge study was also conducted. Figure 6C shows the charge−discharge curves of different electrodes with a potential from −0.8 to 0.2 V. The shape of MG was triangular, indicating pure EDL capacitance. The PPy electrode exhibits a discharging curve consisting of two voltage stages in the ranges of 0.2 to −0.5 V and −0.5 to −0.8 V, implying the pseudocapacitance property. However, the MGPPy showed longer discharge time than the other materials because of the synergistic effect of the conductivity of MG and the pseudocapacitance of PPy. The area specific capacitance of MGPPy was measured to be 196 mF cm^{-2}, which was calculated from the results of charge−discharge curve for the current density of 1 mA cm^{-2}. Compared with other porous electrode materials[51−54] such as onion-like carbon[55] and electrochemically reduced graphene oxide (ErGO)[38] electrode, the MGPPy electrode greatly improved the specific capacitance, which was attributed to the pseudocapacitance of the PPy component. GCD curves of the 120MG120PPy at different current densities are shown in Figure 6D. The linear voltage−time profiles and the symmetric charge−discharge characteristics indicated good capacitive behavior with a rapid $I-V$ response for our asymmetric devices. The charge−discharge with different mass loading of PPy is also shown in Figure S12a. Figure 6E displays the effect of current density on the capacitance values. The MGPPy maintained its 84% capacitance (196 to 165 mF cm^{-2}) as the discharge current density was increased from 1 to 5 mA cm^{-2}. Compared with polypyrrole/sulfonated graphene composite[46] and the PPy/TiO_2/PANI[56] composite electrode, the MGPPy electrode maintained relatively high specific capacitance at large charge/discharge rate, which also confirmed the advantage of the electrode structure. The reason was that the pore walls of the MGPPy were nearly vertical to the surface of the current collector, and thus, micropores in the electrode were exposed to the ions in the electrolyte during the charge and discharge process. Figure S12b shows the impedance spectra of 120MG, 120PPy, 120MG120PPy, and 120MG600PPy, respectively. These images suggested good contact between the MG and PPy, and the increased resistance was mainly attributed to the low conductivity of PPy. Moreover, the 120MG600PPy composite material exhibited an acceptable cycling stability performance over the −0.8 to 0.2 V at a current density of 1 mA cm^{-2} (Figure 6F). The capacitance decreased slightly from 196 to 176 mF cm^{-2} after 500 cycles.

DOI: 10.1021/acsami.5b07982
ACS Appl. Mater. Interfaces 2015, 7, 23731−23740

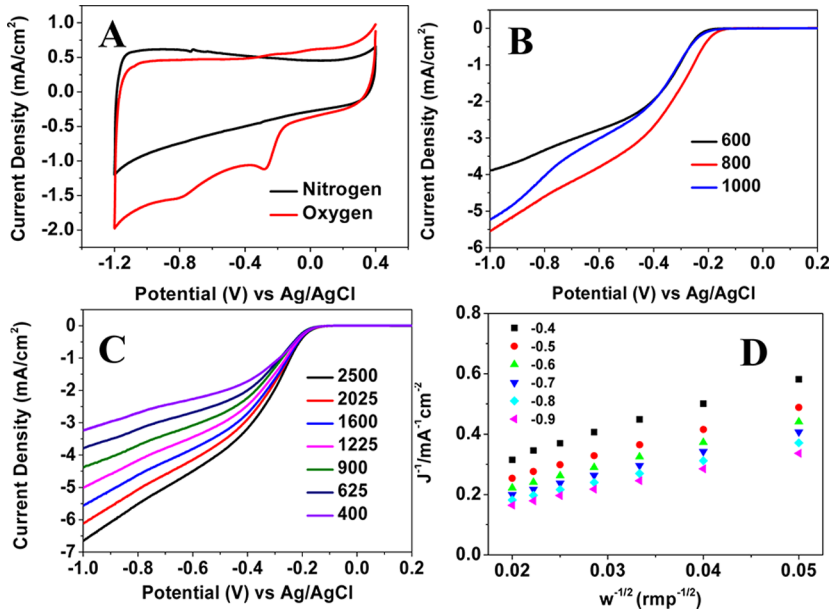

Figure 8. (A) CV curves of the MG and MGPPy-800 electrocatalysts in N_2 and O_2 saturated electrolyte with a scan rate of 50 mV s^{-1}. (B) LSV curves and catalytic activity of MGPPy-600, MGPPy-800, and MGPPy-1000 in O_2 saturated 0.1 M KOH with a scan rate of 10 mV s^{-1} and a rotation rate of 1600 rpm. (C, D) RDE measurement of MGPPy-800 in O_2 saturated 0.1 M KOH with a scan rate of 10 mV s^{-1}. The corresponding Koutecky–Levich plot of J^{-1} versus $\omega^{-1/2}$ from −0.3 to −0.9 V.

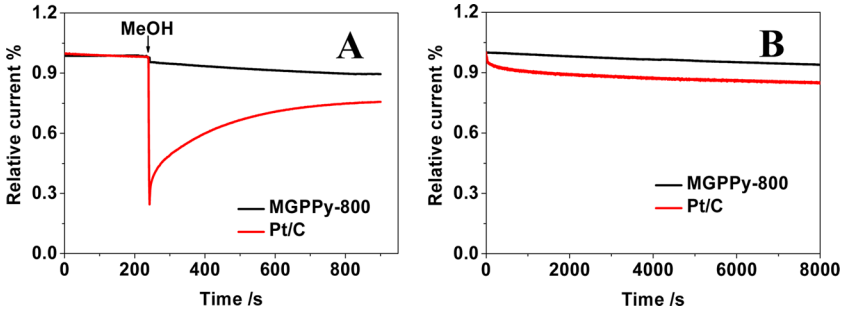

Figure 9. (A) Chronoamperometry of MGPPy-800 and Pt/C electrodes in O_2 saturated 0.1 M KOH at −0.3 V for 8000 s with the rotation rate of 1600 rpm. (B) Chronoamperometric responses of MGPPy-800 and Pt/C electrodes with 3 M methanol added at 240 s with the rotation rate of 1600 rpm.

A symmetric supercapacitor device was prepared by assembling 120MG600PPy based on carbon paper as electrode materials, and the SEM image was shown in Figure S13. Meanwhile, we fabricated the device based on the 120MG600PPy of Au as substrate for comparison (Figure S14). Considering the capacitive properties and economics, carbon paper was chosen as the substrate for devices. The CV of the device at different scan rates from 10 to 300 mV/s is shown in Figure S15. The current intensity increased with the scan rate, and the shape is well retained, indicating its ideal pseudocapacitive nature. Figure 7A showas a GCD test performed at different current densities in the potential window of 0–1.0 V. The linear voltage versus time profiles, the symmetrical charge–discharge characteristics, and a quick $I-V$ response represented good capacitive characteristics for the device. To show the practical application, we assembled three series. As shown in Figure 7B, the device can light the LED red light, indicating high power and energy characteristic of the device.

3.2.2. ORR. As for the catalyst, the novel hierarchical porous structures of the N-doped graphene framework are promising electrode materials which can provide edge-rich planes and large specific surface area with more active sites for ORR in alkaline fuel cells.[57−59] We first examined the electrocatalytic properties of MGPPy-800 in N_2-saturated and O_2-saturated 0.1 M KOH aqueous solution using cyclic voltammetry at a scan rate of 50 mV s^{-1}. In Figure 8A, featureless voltammetry currents within the potential range of −1.0 to +0.2 V were observed for MGPPy-800 in the N_2-saturated solution; in contrast, when the electrolyte was saturated with O_2, an obviously cathodic peak appeared at −0.132 V vs Ag/AgCl, which suggests that MGPPy-800 exhibited electrocatalytic activity for oxygen reduction. In addition, the annealing temperature had a significant impact on the electrochemical performance of N-MGPPy. Among these MGPPy-X, the onset potential for the ORR of MGPPy-800 was more positive than that of MGPPy-600 (−0.187 V) and MGPPy-1000 (−0.179 V) (Figure S16), indicating their high catalytic activity. Subsequently, to examine the reaction kinetics for the MGPPy-800 electrodes, linear sweep voltammograms (LSVs) were recorded in an O_2-saturated 0.1 M KOH electrolyte at a scan rate of 10 mV s^{-1} by using a rotating disk electrode (RDE). The corresponding Koutecky–Levich (K-L) plots were drafted from the ORR polarization curves. Comparing their LSV curves,

DOI: 10.1021/acsami.5b07982
ACS Appl. Mater. Interfaces 2015, 7, 23731−23740

MGPPy-800 showed a superior catalytic activity to samples prepared at other pyrolysis temperatures in view of the onset potential. It has been realized that pyrolysis changes the nitrogen configuration in MGPPy-X, which plays an important role as indicated by the recent report.[60] In fuel cells, a four-electron transfer process of ORR is preferred (Figure S16). The average transferred electron number of MGPPy-800 over the potential range from −0.4 to −0.7 V has been calculated to be increased from 3.21 to 4.06 with the potential on the basis of the ring and disk currents from the RRDE curve.[61,62] Koutecky−Levich plots revealed good linearity between J^{-1} and $\omega^{-1/2}$ and approximately constant slopes over the potentials from −0.4 to −0.9 V. Figures 8D and S17 reveal that the electron transfer number varied strongly with the measured potential. The electron transfer numbers (n) were 3.86 for MGPPy-800, 2.16 for MGPPy-600, and 2.25 for MGPPy-1000 over the potential range of −0.6 V, which indicated that the electrocatalytic process of MGPPy-800 was carried out mainly via a four electron mechanism.

The MGPPy-800 was further subjected to methanol crossover test and the stability for ORR. As shown in Figure 9A, a sharp decrease in the current was observed for the Pt/C electrode upon addition of 3.0 M methanol. However, the corresponding amperometric response for the MGPPy-800 remains almost unchanged. This result explicitly indicates that the MGPPy-800 has higher fuel selectivity toward ORR than the commercial Pt/C electrocatalyst. The stability of MGPPy-800 and Pt/C in O_2-saturated 0.1 M KOH was evaluated by chronoamperomertry at −0.3 V with the electrode rotation rate at 1600 rpm. After 8000 s, the commercial Pt/C catalysts exhibited a loss of 15% of the catalytic activity (Figure 9B) while the MGPPy-800 remained stable throughout the experiment, with only 5.7% of the catalytic activity.

4. CONCLUSION

In summary, we have developed a hydrogen bubble template-directed synthesis method for the fabrication of 3D macroporous graphene-based composite and N-doped graphene modified electrodes. By this approach, hydrogen bubbles arising from the reduction of H^+ function as the dynamic template for graphene electrodeposition. Graphene is electrodeposited in the interstitial spaces between the hydrogen bubbles and forms a 3D macroporous structure on different conducting substrates such as metal foil, carbon paper, and ITO glass. MG has open interconnected macroporous walls and self-supported structures, whose pore size and wall thickness of MG electrode can be tuned by the concentration of surfactants, electrodeposition time, and applied voltage. Meanwhile, we deposited pyrrole monomer on the surface of 3D MG networks, fabricating the MGPPy composite material with good capacity property (196 mF cm^{-2} of 120MG600PPy at the 1 mA cm^{-2}). The asymmetric supercapacitor device assembled by the composite materials has good capacity property, which offers the possible application for real life. After thermal treatment of MGPPy, the obtained N-doped MGPPy electrodes endow the catalyst with excellent catalytic performance toward the ORR. The MGPPy-800 catalyst shows an onset potential of −0.132 V and the highest current density value of 5.56 mA cm^{-2} which involves a four electron pathway. Moreover, the fuel tolerance and durability under the electrochemical environment of the catalyst is found to be superior to the Pt/C catalyst. With the enhanced electrocatalytic activity and durability, this modified electrode turns out to be a potential cost-effective, metal-free electrocatalyst for proton exchange membrane fuel cells (PEMFCs). Compared with some other porous carbon or metal oxide electrode materials, our 3D macroporous graphene composites show advanced electrode properties for the use of supercapacitor electrodes and metal-free electrocatalyst. The reasons are (i) their high surface area and the high conductivity of the graphene network; (ii) high mass transport rate owing to the 3D porous structure; (iii) direct electrode modification through a binder-free procedure.

■ ASSOCIATED CONTENT

Supporting Information

The Supporting Information is available free of charge on the ACS Publications website at DOI: 10.1021/acsami.5b07982.

Characterization and discussion of the GO, MG, MGPPy, and N-MGPPy; SEM, XPS, EDS, Raman, TGA, and BET demonstrating the successful preparation of these composite materials; electrochemical test of composite samples showing the supercapacitor and ORR properties (PDF)

■ AUTHOR INFORMATION

Corresponding Authors

*E-mail: liuar@seu.edu.cn. Fax: 86-25-52090618. Tel: 86-25-52090613.

*E-mail: liusq@seu.edu.cn. Fax: 86-25-52090618. Tel: 86-25-52090613.

Notes

The authors declare no competing financial interest.

■ ACKNOWLEDGMENTS

This work was financially supported by the National Natural Science Foundation of China (21505018), the Natural Science Foundation of Jiangsu Province of China (BK 20141348), and the Fundamental Research Funds for the Central Universities.

■ REFERENCES

(1) Novoselov, K. S.; Geim, A. K.; Morozov, S. V.; Jiang, D.; Zhang, Y.; Dubonos, S. V.; Grigorieva, I. V.; Firsov, A. A. Electric Field Effect in Atomically Thin Carbon Films. *Science* **2004**, *306*, 666−669.

(2) Nair, R. R.; Blake, P.; Grigorenko, A. N.; Novoselov, K. S.; Booth, T. J.; Stauber, T.; Peres, N. M. R.; Geim, A. K. Fine Constant Defines Visual Transparency of Graphene. *Science* **2008**, *320*, 1308.

(3) Lee, C. G.; Wei, X. D.; Kysar, J. W.; Hone, J. Measurement of the Elastic Properties and Intrinsic Strength of Monolayer Graphene. *Science* **2008**, *321*, 385−388.

(4) Stoller, M. D.; Park, S.; Zhu, Y. W.; An, J. H.; Ruoff, R. S. Graphene-Based Ultracapacitors. *Nano Lett.* **2008**, *8*, 3498−3502.

(5) Huang, X.; Qi, X.; Boey, F.; Zhang, H. Graphene-Based composites. *Chem. Soc. Rev.* **2012**, *41*, 666−686.

(6) Pumera, M. Graphene-Based Nanomaterials for Energy Storage. *Energy Environ. Sci.* **2011**, *4*, 668−674.

(7) Liang, M. H.; Zhi, L. J. Graphene-Based Electrode Materials for Rechargeable Lithium Batteries. *J. Mater. Chem.* **2009**, *19*, 5871−5878.

(8) Zhang, L. L.; Zhou, R.; Zhao, X. S. Graphene-Based Materials as Supercapacitor Electrodes. *J. Mater. Chem.* **2010**, *20*, 5983−5992.

(9) Xiao, J.; Mei, D.; Li, X.; Xu, W.; Wang, D.; Graff, G. L.; Bennett, W. D.; Nie, Z.; Saraf, L. V.; Aksay, I. A.; Liu, J.; Zhang, J. G. Hierarchically Porous Graphene as A Lithium-Air Battery Electrode. *Nano Lett.* **2011**, *11*, 5071−5078.

(10) Yoo, E.; Zhou, H. S. Li-Air Rechargeable Battery Based on Metal-Free Graphene Nanosheet Catalysts. *ACS Nano* **2011**, *5*, 3020−3026.

DOI: 10.1021/acsami.5b07982
ACS Appl. Mater. Interfaces 2015, 7, 23731−23740

(11) Shao, Y. Y.; Wang, J.; Wu, H.; Liu, J.; Aksay, I. A.; Lin, Y. H. Graphene Based Electrochemical Sensors and Biosensors: A Review. *Electroanalysis* **2010**, *22*, 1027−1036.
(12) Chen, D.; Tang, L. H.; Li, J. H. Graphene-Based Materials in Electrochemistry. *Chem. Soc. Rev.* **2010**, *39*, 3157−3180.
(13) Wei, W.; Yang, S. B.; Zhou, H. X.; Lieberwirth, I.; Feng, X. L.; Mullen, K. 3D Graphene Foams Cross-Linked with Pre-Encapsulated Fe_3O_4 Nanospheres for Enhanced Lithium Storage. *Adv. Mater.* **2013**, *25*, 2909−2914.
(14) Luo, J. S.; Liu, J. L.; Zeng, Z. Y.; Ng, C. F.; Ma, L. J.; Zhang, H.; Lin, J. Y.; Shen, Z. X.; Fan, H. J. Three-Dimensional Graphene Foam Supported Fe_3O_4 Lithium Battery Anodes with Long Cycle Life and High Rate Capability. *Nano Lett.* **2013**, *13*, 6136−6143.
(15) Gong, Y. J.; Yang, S. B.; Liu, Z.; Ma, L. L.; Vajtai, R.; Ajayan, P. M. Graphene-Network-Backboned Architectures for High-Performance Lithium Storage. *Adv. Mater.* **2013**, *25*, 3979−3984.
(16) Unni, S. M.; Devulapally, S.; Karjule, N.; Kurungot, S. Graphene Enriched with Pyrrolic Coordination of the Doped Nitrogen as an Efficient Metal-Free Electrocatalyst for Oxygen Reduction. *J. Mater. Chem.* **2012**, *22*, 23506−23513.
(17) Zhu, Y.; Murali, S.; Stoller, M. D.; Ganesh, K. J.; Cai, W.; et al. Carbon-Based Supercapacitors Produced by Activation of Graphene. *Science* **2011**, *332*, 1537−1541.
(18) Xu, Y. X.; Bai, H.; Lu, G. W.; Li, C.; Shi, G. Q. Flexible Graphene Films via the Filtration of Water-Soluble Noncovalent Functionalized Graphene Sheets. *J. Am. Chem. Soc.* **2008**, *130*, 5856−5857.
(19) Xu, Y. X.; Shi, G. Q.; Duan, X. F. Self-Assembled Three-Dimensional Graphene Macrostructures: Synthesis and Applications in Supercapacitors. *Acc. Chem. Res.* **2015**, *48*, 1666−1675.
(20) Li, C.; Shi, G. Q. Three-Dimensional Graphene Architectures. *Nanoscale* **2012**, *4*, 5549−5563.
(21) Niu, Z.; Du, J.; Cao, X.; et al. Electrophoretic Buildup of Alternately Multilayered Films and Micro-patterns Based on Graphene Sheets and Nanoparticles and Their Applications in Flexible Supercapacitors. *Small* **2012**, *8*, 3201−3208.
(22) Li, C.; Shi, G. Q. Functional Gels Based on Chemically Modified Graphenes. *Adv. Mater.* **2014**, *26*, 3992−4012.
(23) Cao, X. H.; Yin, Z. Y.; Zhang, H. Three-dimensional Graphene Materials: Preparation, Structures and Application in Supercapacitors. *Energy Environ. Sci.* **2014**, *7*, 1850−1865.
(24) Zhu, J.; Yin, Z.; Li, H.; Tan, H.; Chow, C. H.; Zhang, H.; Hng, H. H.; Ma, J.; Yan, Q. Bottom-Up Preparation of Porous Metal Oxides Ultrathin Sheets with Adjustable Composition/Phases and Their Applications. *Small* **2011**, *7*, 3458−3464.
(25) Chen, Z. P.; Ren, W. C.; Gao, L. B.; Liu, B. L.; Pei, S. F.; Cheng, H. M. Three-Dimensional Flexible and Conductive Interconnected Graphene Networks Grown by Chemical Vapour Deposition. *Nat. Mater.* **2011**, *10*, 424−428.
(26) Xia, X. H.; Chao, D. L.; Fan, Z. X.; Guan, C.; Cao, X. H.; Zhang, H.; Fan, H. J. A New Type of Porous Graphite Foams and Their Integrated Composites with Oxide/Polymer Core/Shell Nanowires for Supercapacitors: Structural Design, Fabrication, and Full Supercapacitor Demonstrations. *Nano Lett.* **2014**, *14*, 1651−1658.
(27) Li, N.; Chen, Z.; Ren, W.; Li, F.; Cheng, H. M. Flexible Graphene-Based Lithium Ion Batteries with Ultrafast Charge and Discharge Rates. *Proc. Natl. Acad. Sci. U. S. A.* **2012**, *109*, 17360.
(28) Huang, X. D.; Qian, K.; Yang, J.; Zhang, J.; Li, L.; Yu, C. Z.; Zhao, D. Y. Functional Nanoporous Graphene Foams with Controlled Pore Sizes. *Adv. Mater.* **2012**, *24*, 4419−4423.
(29) Choi, B. G.; Chang, S. J.; Lee, Y. B.; Bae, J. S.; Kim, H. J.; Huh, Y. S. 3D Heterostructured Architectures of Co_3O_4 Nanoparticles Deposited on Porous Graphene Surfaces for High Performance of Lithium Ion Batteries. *Nanoscale* **2012**, *4*, 5924−5930.
(30) Choi, B. G.; Yang, M.; Hong, W. H.; Choi, J. W.; Huh, Y. S. 3D Macroporous Graphene Frameworks for Supercapacitors with High Energy and Power Densities. *ACS Nano* **2012**, *6*, 4020−4028.
(31) Zhou, X. S.; Yin, Y. X.; Cao, A. M.; Wan, L. J.; Guo, Y. G. Efficient 3D Conducting Networks Built by Graphene Sheets and Carbon Nanoparticles for High-Performance Silicon Anode. *ACS Appl. Mater. Interfaces* **2012**, *4*, 2824−2828.
(32) Shao, Y. Y.; Zhang, S.; Engelhard, M. H.; Li, G. S.; Shao, G. C.; Wang, Y.; Liu, J.; Aksay, L. A.; Lin, Y. H. Nitrogen-Doped Graphene and Its Electrochemical Applications. *J. Mater. Chem.* **2010**, *20*, 7491−7496.
(33) Ahn, H. S.; Jang, J. W.; Seol, M.; Kim, J. M.; Yun, D. J.; Park, C.; Kim, H.; Youn, D. H.; Kim, J. Y.; Park, G.; Park, S. C.; Kim, J. M.; Yu, D. I.; Yong, K. J.; Kim, M. H.; Lee, J. S. Self-Assembled Foam-like Graphene Networks Formed through Nucleate Boiling. *Sci. Rep.* **2013**, *3*, 1396.
(34) Azevedo, J. l.; Costa-Coquelard, C.; Jegou, P.; Yu, T.; Benattar, J. J. Highly Ordered Monolayer, Multilayer, and Hybrid Films of Graphene Oxide Obtained by the Bubble Deposition Method. *J. Phys. Chem. C* **2011**, *115*, 14678−14681.
(35) Li, Y.; Jia, W. Z.; Song, Y. Y.; Xia, X. H. Superhydrophobicity of 3D Porous Copper Films Prepared Using the Hydrogen Bubble Dynamic Template. *Chem. Mater.* **2007**, *19*, 5758−5764.
(36) Tokuno, T.; Nogi, M.; Jiu, J. T.; Sugahara, T.; Suganuma, K. Transparent Electrodes Fabricated via the Self-Assembly of Silver Nanowires Using a Bubble Template. *Langmuir* **2012**, *28*, 9298−9302.
(37) Xu, Y. X.; Sheng, K. X.; Li, C.; Shi, G. Q. Self-Assembled Graphene Hydrogel via a One-Step Hydrothermal Process. *ACS Nano* **2010**, *4*, 4324−4330.
(38) Sheng, K. X.; Sun, Y. Q.; Li, C.; Yuan, W. J.; Shi, G. Q. Ultrahigh-Rate Supercapacitors Based on Eletrochemically Reduced Graphene Oxide for Ac Line-Filtering. *Sci. Rep.* **2012**, *2*, 247.
(39) Qu, L. T.; Shi, G. Q.; Yuan, J. Y.; Han, G. Y.; Chen, F. E. Preparation of Polypyrrole Microstructures by Direct Electrochemical Oxidation of Pyrrole in an Aqueous Solution of Camphorsulfonic Acid. *J. Electroanal. Chem.* **2004**, *561*, 149−156.
(40) Li, D.; Muller, M. B.; Gilje, S.; Kaner, R. B.; Wallace, G. G. Processable Aqueous Dispersions of Graphene Nanosheets. *Nat. Nanotechnol.* **2008**, *3*, 101−105.
(41) Zhang, L. J.; Zhang, X. H.; Fan, C. H.; Zhang, Y.; Hu, J. Nanoscale Multiple Gaseous Layers on a Hydrophobic Surface. *Langmuir* **2009**, *25*, 8860−8864.
(42) Kulkarni, A. A.; Joshi, J. B. Bubble Formation and Bubble Rise Velocity in Gas-Liquid Systems: A Review. *Ind. Eng. Chem. Res.* **2005**, *44*, 5873−5931.
(43) Zhao, L.; Tong, L.; Li, C.; Gu, Z.; Shi, G. Q. Polypyrrole Actuators with Inverse Opal Structures. *J. Mater. Chem.* **2009**, *19*, 1653−1658.
(44) Zhang, J.; Yu, Y.; Liu, L.; Wu, Y. Graphene-Hollow PPy Sphere 3D-Nanoarchitecture with Enhanced Electrochemical Performance. *Nanoscale* **2013**, *5*, 3052−3057.
(45) Wang, Y. H.; Bian, K.; Hu, C. G.; Zhang, Z. P.; Chen, N.; Zhang, H. M.; Qu, L. T. Flexible and Wearable Graphene/Polypyrrole Fibers towards Multifunctional Actuator Applications. *Electrochem. Commun.* **2013**, *35*, 49−52.
(46) Liu, A. R.; Li, C.; Bai, H.; Shi, G. Q. Electrochemical Deposition ofPolypyrrole/Sulfonated Graphene Composite Films. *J. Phys. Chem. C* **2010**, *114*, 22783−22789.
(47) Zhou, H. H.; Han, G. Y.; Xiao, Y. M.; Chang, Y. Z.; Zhai, H. J. Facile Preparation of Polypyrrole/Graphene Oxide Nanocomposites with Large Areal Capacitance using Electrochemical Codeposition for Supercapacitors. *J. Power Sources* **2014**, *263*, 259−267.
(48) Feng, X. M.; Zhang, Y.; Zhou, J. H.; Li, Y.; Chen, S. F.; Zhang, L.; Ma, Y. W.; Wang, L. H.; Yan, X. H. Three-Dimensional Nitrogen-Doped Graphene as an Ultrasensitive Electrochemical Sensor for the Detection of Dopamine. *Nanoscale* **2015**, *7*, 2427−2432.
(49) Lin, Z. Y.; Waller, G. H.; Liu, Y.; Liu, M. L.; Wong, C. P. 3D Nitrogen-Doped Graphene Prepared by Pyrolysis of Graphene Oxide with Polypyrrole for Electrocatalysis of Oxygen Reduction Reaction. *Nano Energy* **2013**, *2*, 241−248.
(50) Wu, G.; Mack, N. H.; Gao, W.; Ma, S. G.; Zhong, R. Q.; Han, J. T.; Baldwin, J. K.; Zelenay, P. Nitrogen Doped Graphene-Rich Catalysts Derived from Heteroatom Polymers for Oxygen Reduction

DOI: 10.1021/acsami.5b07982
ACS Appl. Mater. Interfaces 2015, 7, 23731−23740

in Nonaqueous Lithium-O_2 Battery Cathodes. *ACS Nano* **2012**, *6*, 9764−9776.
(51) Meng, Y. N.; Zhao, Y.; Hu, C. G.; Cheng, H. H.; Hu, Y.; Zhang, Z. P.; Shi, G. Q.; Qu, L. T. All-Graphene Core-Sheath Microfibers for All-Solid-State, Stretchable Fibriform Supercapacitors and Wearable Electronic Textiles. *Adv. Mater.* **2013**, *25*, 2326−2331.
(52) Wu, Z. S.; Sun, Y.; Tan, Y. Z.; Yang, S. B.; Feng, X. L.; Müllen, K. Three-Dimensional Graphene-Based Macro- and Mesoporous Frameworks for High-Performance Electrochemical Capacitive Energy Storage. *J. Am. Chem. Soc.* **2012**, *134*, 19532−19535.
(53) Peng, C.; Zhou, X. H.; Zhang, S. W.; Ng, K. C.; Chen, G. Z. Recent Advances in Supercapacitors with Nanocomposite Electrodes. *ECS Trans.* **2011**, *33*, 107−116.
(54) Kim, T. Y.; Jung, G. J.; Yoo, S.; Suh, K. S.; Ruoff, R. S. Activated Graphene-Based Carbons as Supercapacitor Electrodes with Macro- and Mesopores. *ACS Nano* **2013**, *7*, 6899−6905.
(55) Pech, D.; Brunet, M.; Durou, H.; Huang, P.; Mochalin, V.; Gogotsi, Y.; Taberna, P. L.; Simon, P. Ultrahigh-Power Micrometre-Sized Supercapacitors Based on Onion-like Carbon. *Nat. Nanotechnol.* **2010**, *5*, 651−654.
(56) Xie, Y. B.; Wang, D.; Zhou, Y. Z.; Du, H. X.; Xia, C. Supercapacitance of Polypyrrole/Titania/Polyanilinecoaxial Nanotube Hybrid. *Synth. Met.* **2014**, *198*, 59−66.
(57) Wang, J.; Wang, H. S.; Wang, K.; Wang, F. B.; Xia, X. H. Ice Crystals Growth Driving Assembly of Porous Nitrogen-Doped Graphene for Catalyzing Oxygen Reduction Probed by in Situ Fluorescence Electrochemistry. *Sci. Rep.* **2014**, *4*, 6723.
(58) Sheng, Z. H.; Shao, L.; Chen, J. J.; Bao, W. J.; Wang, F. B.; Xia, X. H. Catalyst-Free Synthesis of Nitrogen-Doped Graphene via Thermal Annealing Graphite Oxide with Melamine and Its Excellent Electrocatalysis. *ACS Nano* **2011**, *5*, 4350−4358.
(59) Sheng, Z. H.; Gao, H. L.; Bao, W. J.; Wang, F. B.; Xia, X. H. Synthesis of Boron Doped Graphene for Oxygen Reduction Reaction in Fuel Cells. *J. Mater. Chem.* **2012**, *22*, 390−395.
(60) Zheng, B.; Wang, J.; Wang, F. B.; Xia, X. H. Synthesis of Nitrogen Doped Graphene with High Electrocatalytic Activity toward Oxygen Reduction Reaction. *Electrochem. Commun.* **2013**, *28*, 24−26.
(61) Silva, R.; Voiry, D.; Chhowalla, M.; Asefa, T. Efficient Metal-Free Electrocatalysts for Oxygen Reduction: Polyaniline-Derived N- and O-Doped Mesoporous Carbons. *J. Am. Chem. Soc.* **2013**, *135*, 7823−7826.
(62) Li, Y.; Zhao, Y.; Cheng, H. H.; Hu, Y.; Shi, G. Q.; Dai, L. M.; Qu, L. T. Nitrogen-Doped Graphene Quantum Dots with Oxygen-Rich Functional Groups. *J. Am. Chem. Soc.* **2012**, *134*, 15−18.

DOI: 10.1021/acsami.5b07982
ACS Appl. Mater. Interfaces 2015, 7, 23731−23740